Applied Research

RESEARCH ARTICLE OPEN ACCESS

Oligochitosan Conjugates of the Antimalarials Dihydroartemisinin and Lumefantrine: Synthesis, Stability, Cell Viability, and Antiplasmodial Studies

William Matshe[1] | Sindisiwe Mvango[1,2†] | Rudzani Malabi[1] | Asongwe Tantoh[3] | Charlene Andraos[4] | Ibukun Famuyide[5] | Lyndy McGaw[5] | Sooraj Baijnath[6] | Lynne Pilcher[2] | Mohammed Balogun[1]

[1]Biopolymer Modification and Advanced Therapeutics Laboratory, Centre for Nanostructured and Advanced Materials, Chemicals Cluster, Council for Scientific and Industrial Research, Pretoria, South Africa | [2]Department of Chemistry, University of Pretoria, Pretoria, South Africa | [3]Pharmaceutical Technologies, Chemicals Cluster, Council for Scientific and Industrial Research, Pretoria, South Africa | [4]Toxicology and Biochemistry department, National Institute for Occupational Health, National Health Laboratory Service, Johannesburg, South Africa | [5]Phytomedicine Programme, Department of Paraclinical Sciences, Faculty of Veterinary Science, University of Pretoria, Pretoria, South Africa | [6]Wits Integrated Molecular Physiology Research Initiative, Wits Health Consortium, Department of Physiology, School of Biomedical Sciences, Faculty of Health Sciences, University of the Witwatersrand, Johannesburg, South Africa

Correspondence: Mohammed Balogun (mohammedbalogun@tuks.co.za)

Received: 29 March 2025 | **Revised:** 1 September 2025 | **Accepted:** 17 September 2025

Keywords: antimalarials | artemisinins | biopolymers | conjugates | delivery systems | lumefantrine | oligochitosan

ABSTRACT

Malaria is treatable with several combinations of drugs, the most well-known and currently most effective being artemisinin-based therapies. Gastrointestinal absorption of these drugs can be poor and erratic if not taken with a fatty meal. Nausea and the loss of appetite, common symptoms of even mild malaria, can therefore jeopardize the effectiveness of the treatment. To enhance the bioavailability of artemisinin-based combination therapies, several lipid-based formulations and delivery systems have been investigated. In this study, we synthesized oligochitosan conjugates of the antimalarial drugs dihydroartemisinin and lumefantrine and examined their physical stability and biological activities. The hydrodynamic properties of both conjugates varied unpredictably under pH conditions like those found at different stages along the gastrointestinal tract and in plasma. The viability of Caco-2 cells exposed to the conjugates was also investigated in comparison to the free drugs. Both conjugates demonstrated significantly lower cytotoxicity compared to the free drugs at concentrations up to 0.5 mg/mL, particularly during the first 24 h of exposure. Despite this, they retained their antiplasmodial effect against *Plasmodium falciparum* in an in vitro assay at 1 μg/mL and 5 μg/mL. These new chitosan biomaterials hold great potential for further development into oral therapeutics that would not require fatty meal intake due to the intrinsic mucoadhesiveness of chitosan.

1 | Introduction

Malaria is a parasitic infectious disease transmitted by the female *Anopheles* mosquito when she takes a blood meal for the development of her eggs. The infectious agent is the protozoan *Plasmodium*, which has a life cycle split between the mosquito and humans [1]. Of the five species that infect humans, *Plasmodium falciparum* causes the severest disease. It is responsible for over 99% of all cases on the African continent, which bears more than 90% of global malaria infections and deaths [2]. In malaria-endemic regions, most adult cases do not require hospitalization due to some level of immunity acquired from

Abbreviations: C_{max}, maximum plasma concentration; MWCO, molecular weight cutoff; SD, standard deviation; SEM, standard error of mean.

†Sindisiwe Mvango deceased on 26 April 2024.

repeated exposures. These cases are typically treatable with oral combination therapies that are based on derivatives of phytochemical artemisinin [3].

Artemisinin is a sesquiterpene lactone derived from the *Artemisia annua* plant, commonly known as sweet wormwood [4]. Artemisinin-based drugs are currently the most effective treatments approved for the disease [3, 5]. However, artemisinin itself is not preferred in clinical practice as an antimalarial due to its poor aqueous solubility (approximately 61.83 mg/L), which limits its bioavailability and effectiveness. Synthetic artemisinin derivatives with improved aqueous solubility commonly used in malaria treatment include dihydroartemisinin (DHA), artemether (Art), arteether, and artesunate [6]. These drugs have a rapid onset of action but are almost as rapidly cleared from the systemic circulation with maximum plasma half-lives of only a couple of hours. A second drug with a much longer plasma elimination half-life is recommended in artemisinin-based combination therapy (ACT), the current gold standard regimen for treating the disease. Common partner drugs include lumefantrine (Lumf), piperaquine, mefloquine, and amodiaquine [3].

ACTs are primarily administered orally. These drugs have substantial lipophilicity that enhances their penetration of tissues and the blood–brain barrier but also presents a challenge for gastrointestinal uptake [7, 8]. The poor aqueous solubility of these drugs poses challenges for dissolution in the aqueous intestinal lumen and crossing the unstirred water layer to reach the mucosal membrane.

To improve absorption and bioavailability, it is often recommended that the drugs are taken together with a fatty meal [9]. In a study of 12 healthy adult volunteers, intake of 36 mL of soya milk with a fat content of about 1.2 g increased the plasma concentration of Lumf by fivefold [10]. The fat is believed to stimulate the production of bile salts, which aid in the emulsification and absorption of the lipidic drug.

Although only a small amount of fat is needed to significantly improve absorption and bioavailability, the anorexia and emesis frequently associated with malaria can cause considerable variations in the oral bioavailability of ACTs. Children, who are the most vulnerable to the disease, are also more likely to refuse or be unable to hold down a meal during the acute phase of malarial infection. These challenges have spurred research into developing advanced formulations and delivery systems for ACT drugs [1, 11].

Lipid nanocarriers have been studied for the delivery of ACTs, with solid lipid nanoparticles (SLNs) and nanostructured lipid carriers (NLCs) being the most studied [12]. These two delivery systems primarily differ in the phase of their lipid cores: SLNs have a core of solid lipids, while NLCs contain a core composed of a mixture of solid and liquified lipids [13]. NLCs are considered an advancement over SLNs due to their higher drug loading capacity and greater stability.

Odera et al. formulated DHA and Lumf into SLNs [14]. These SLNs were reported to release their drug payload over 72 h, resulting in a 31% improvement in therapeutic efficacy in *Plasmodium berghei*-infected mice. Another study involved the formulation of SLNs of Lumf alone. A 2.7- and 2.2-fold increase in plasma C_{max} and area under the curve (AUC) was observed, respectively, compared to the unformulated drug after oral administration to mice [15]. The improvement in bioavailability was attributed to the faster dissolution rate of the formulated Lumf.

NLCs of the fixed-dose combination of Art-Lumf have also been developed for both oral and intravenous administration using an industrially feasible microemulsion technique [16, 17]. The oral NLC demonstrated efficacy in *P. berghei*-infected mice at one-tenth the dose of the unformulated combination.

Although less explored, biomaterials offer an attractive non-lipid-based alternative system for ACT delivery, potentially enabling simpler therapeutic formulations [18]. These materials are programmable and highly efficient for drug delivery, with finely tunable release profiles. Chitosan (Cs), a derivative of the naturally occurring biopolymer chitin, is a major polysaccharide component of edible crustacean shells, insect exoskeletons, and fungal cell walls. It is obtained through partial chemical or enzymatic deacetylation of chitin. With $\beta(1\rightarrow4)$ glycosidic bonds between acetylated and deacetylated glucosamine monomeric units, Cs is enzymatically nondegradable in the human digestive tract but may be degradable by intracellular lysosomal enzymes, with highly deacetylated low-molecular-weight Cs being more susceptible to enzymatic degradation [19].

Despite decades of intensive study, new biomaterials continue to be developed based on this highly versatile polymer [20, 21]. Remarkably, as new needs emerge, it seems possible to develop a Cs-based solution. Garcia et al. recently reported the co-formulation of a Cs derivative, chitosan-*N*-arginine, in a polymer–lipid hybrid nanoparticle system for mRNA delivery [22].

Cs is inherently cationic due to its free primary amine group, which is responsible for the mucoadhesive property of the polymer. This property has been exploited for drug delivery systems' uptake through the opening of tight junctions in the intestinal epithelium [23, 24]. Recently, Gomes et al. reported on Cs nanoparticles loaded with the antimalarial drug primaquine, co-formulated with D-galactose as a liver-targeting ligand [25]. A significant increase in liver accumulation of primaquine was observed in mice administered the formulation orally. Additionally, a vanillin-crosslinked Cs-polyvinyl alcohol film containing the drug enrofloxacin was demonstrated as a transdermal drug delivery system without the use of permeability enhancers [26].

Apart from the numerous primary amine groups, Cs is also polyhydric. Each deacetylated glucosamine residue has two free hydroxyl groups for every free amine group. The better nucleophilicity of the amine group makes it a preferential target for chemical modifications [26–30]. This has spurred research into Cs as a polymeric carrier of conjugated drugs [31]. The anticancer drugs paclitaxel and docetaxel were conjugated to low-molecular-weight Cs via a labile succinic acid linker for oral delivery [32, 33]. These Cs–paclitaxel and Cs–docetaxel

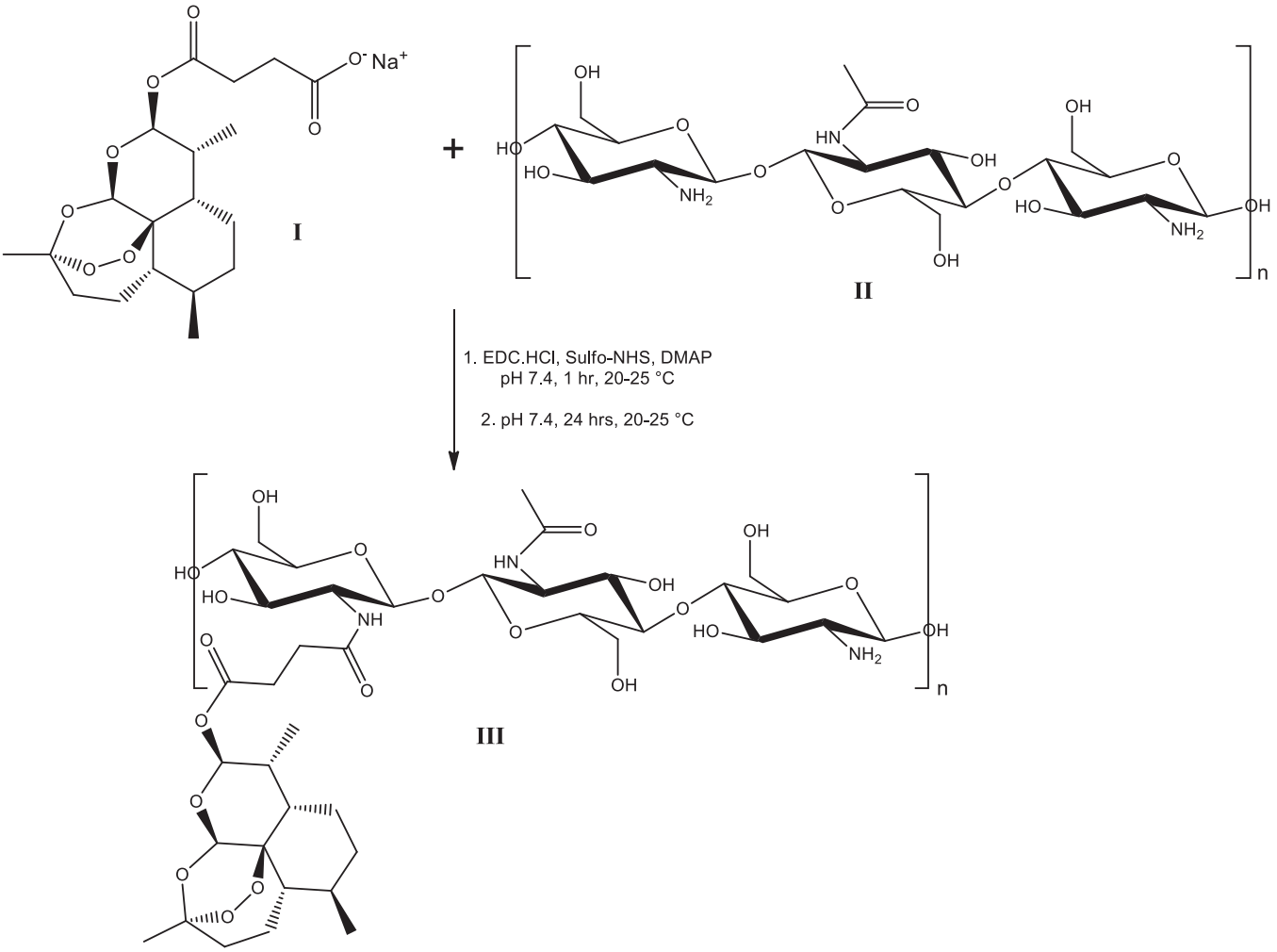

SCHEME 1 | Synthesis of OC–DHA conjugate. A schematic representation of the conjugation of DHA-Suc to OC (I = DHA-Suc; II = OC; III = OC–DHA conjugate).

conjugates exhibited increased aqueous solubility, prolonged gastrointestinal retention due to the polymer's mucoadhesiveness, and enhanced drug bioavailability. Low-molecular-weight Cs (< 10 kDa) has higher intestinal absorption profiles and lower cytotoxicity than high molecular weight Cs [34].

However, the application of polymer–drug conjugation delivery systems to malaria has been very limited [1, 35–37]. Previous polymer-conjugated systems were designed for parenteral administration. Xiao et al. synthesized a Cs–artemisinin conjugate, demonstrating increased drug solubility but without investigating its biological activity [38]. Here, we report on the synthesis, stability, and cytotoxicity of low-molecular-weight Cs-based conjugates of DHA and Lumf for potential further development as oral antimalarial therapeutics.

2 | Materials and Methods

Oligochitosan (OC; molecular weight: < 3 kDa, degree of deacetylation: 93%) (Figure S1), DHA-hemisuccinic acid (DHA-Suc), and Lumf were purchased from DB Fine Chemicals Pty Ltd (South Africa). Dimethylformamide (DMF), succinic anhydride, dimethylaminopyridine (DMAP), *N*-ethyl-*N*-(3-dimethylaminopropyl) carbodiimide hydrochloride (EDC•HCl), *N,N′*-diisopropylcarbodiimide (DIC), *N*-hydroxysuccinimide (NHS), sulfo-*N*-hydroxysuccinimide (sulfo-NHS), diisopropylethylamine (DIEA), dichloromethane (DCM), deuterated dimethyl sulfoxide (d-DMSO), deuterium oxide (D_2O), ethyl acetate (EtOAc), hexane, and sodium bicarbonate ($NaHCO_3$) were all purchased from Sigma-Aldrich (South Africa) and CRD Chemicals Pty Ltd (South Africa). In vitro biology assay consumables were purchased from Merck Ltd (South Africa), Whitehead Scientific Pty Ltd (South Africa), African Oxygen Ltd (South Africa), and American Type Culture Collection organization (ATCC, the United States).

Proton nuclear magnetic resonance (^{1}H NMR) spectra were measured on the Bruker 400 MHz instrument at 295.4 K. Infrared absorption spectra were measured using the Perkin Elmer Spectrum 100 Fourier Transform Infrared (FTIR) Spectrometer.

2.1 | Synthesis

2.1.1 | Synthesis of OC–DHA Conjugate

To a stirring suspension of DHA-Suc (517 mg, 1.2 mol eqv) in phosphate-buffered saline (PBS, pH 7.4, 10 mL), a

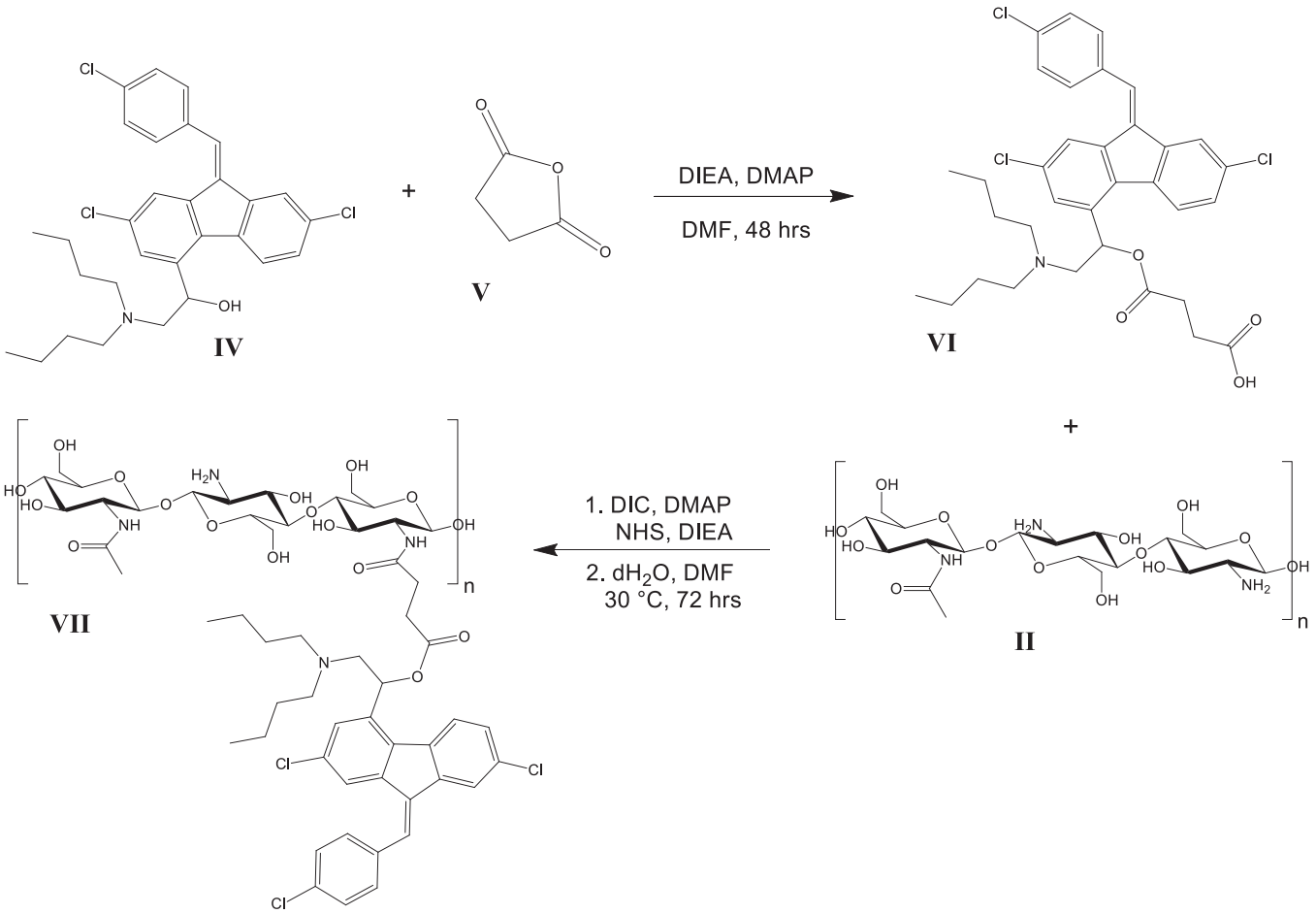

SCHEME 2 | Synthesis of OC–Lumf conjugate (IV = Lumf; V = succinic anhydride; VI = Lumf-Suc; II = OC; VII = OC–Lumf conjugate).

concentrated solution of sodium bicarbonate was added dropwise until the acid was completely dissolved and no further effervescence occurred. EDC•HCl (3.6 mol eqv) and NHS (3.6 mol eqv) were then added at room temperature (20°C–25°C) to activate the DHA-Suc (Scheme 1). After 1 h, the solution of activated DHA-Suc was added dropwise to a stirring solution of OC (500 mg, 1.0 mol eqv) in PBS (10 mL), and the reaction was allowed to proceed for 24 h at room temperature. The reaction mixture was dialyzed using a PUR-A-LYZER kit (MWCO: 1 kDa) for 72 h. The purified OC–DHA product was obtained as a powder with a 90% yield after lyophilization.

2.1.2 | Synthesis of OC–Lumf Conjugate

2.1.2.1 | Synthesis of Lumf-Hemisuccinic Acid (Lumf-Suc). A solution of Lumf (1.0 g, 1.0 mol eqv) and DMAP (0.01 mol eqv) in DMF (12.0 mL) was stirred at 35°C (Scheme 2). Succinic anhydride (1.5 mol eqv) was added to the reaction mixture and monitored by TLC. After 24 h, the solvent was removed in vacuo, yielding a dark-yellow slurry. The crude product was purified by flash column chromatography on a Teledyne NextGen CombiFlash 300$^+$ using hexane:EtOAc (1:3) as the mobile phase. The pure Lumf-Suc product was obtained as a yellow powder with a 95% yield after solvent evaporation.

2.1.2.2 | Conjugation of Lumf-Suc to OC. A solution of Lumf-Suc (220.50 mg, 1.4 mol eqv) in DMF (10 mL) was activated with DIC, NHS, and DMAP and stirred at 35°C for 2 h. The activated Lumf-Suc solution was then added dropwise to a solution of OC (750 mg, 1.0 mol eqv) in a water:DMF (1:3, 50 mL) solvent mixture basified with DIEA (< 1% v/v). The reaction mixture was stirred for 72 h. The crude product was washed three times with acetone by low-speed centrifugation and dried in vacuo at 300 mbar to obtain the pure OC–Lumf product as a free-flowing powder at 98% product yield.

2.2 | Hydrodynamic Properties

The hydrodynamic properties of the conjugates were assessed using dynamic light scattering (DLS) on a Malvern Panalytical Zetasizer (the United Kingdom) in simulations of the varying gastrointestinal tract (GIT) pH conditions. Solutions of OC–DHA (2.5 mg/mL) and OC–Lumf (2.5 mg/mL) were initially prepared at pH 7.4 and 1.3 and incubated at 37°C. The pH 7.4 solutions were analyzed immediately without further pH adjustments. For the pH 1.3 solutions, the pH was raised to 6.5 with aqueous NaOH after 1 h and incubated at 37°C until the 16-h time point, when samples were taken for DLS analysis. The pH was then adjusted to 7.4 with aqueous NaOH and incubated at 37°C until the 48-h time point for the final DLS analysis.

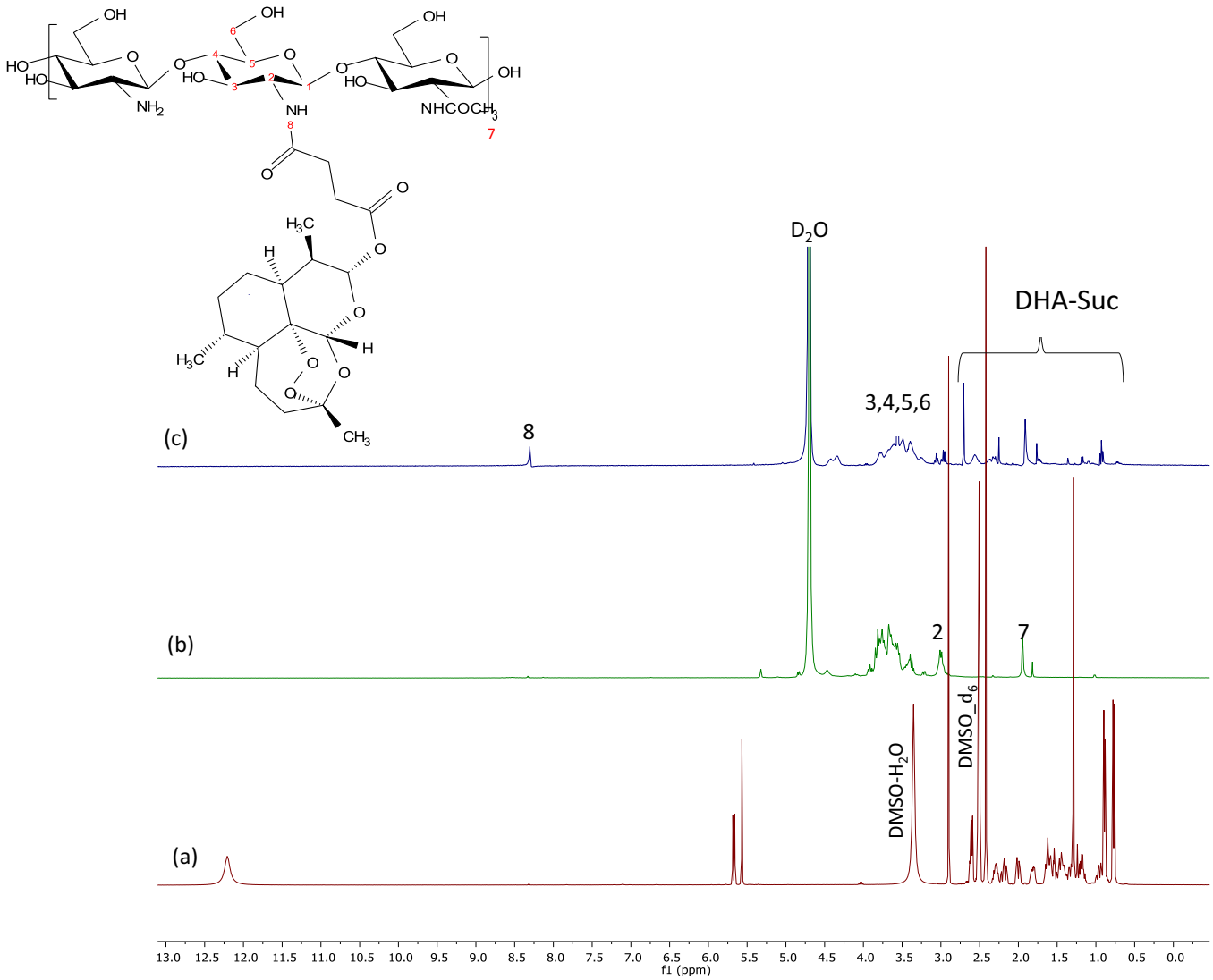

FIGURE 1 | ^{1}H NMR spectra of (a) DHA, (b) OC, and (c) OC–DHA. Spectrum (a) was run in DMSO-d_6, while (b) and (c) were run in D_2O (400 MHz).

All samples were filtered through 0.45 μm syringe filters before DLS analysis. A refractive index of 1.520 and an absorption value of 0.001 were used to determine the hydrodynamic properties of the drug conjugates.

2.3 | In Vitro Cytotoxicity Assessment

2.3.1 | Caco-2 Cytotoxicity

The cytotoxicity of OC conjugates was evaluated in human colon adenocarcinoma (Caco-2) cells. Cells were cultured in Dulbecco's Modified Eagle Medium (DMEM) supplemented with 10% fetal bovine serum, 1% penicillin-streptomycin, and 20 mM $NaHCO_3$ in a humidified incubator at 37°C with 5% CO_2. Cells were seeded at a density of 5×10^3 cells/well in 96-well plates and incubated for 24 h.

Stock solutions of free DHA (10 mg/mL) and Lumf (10 mg/mL) were prepared in DMSO, while OC–DHA (2 mg/mL) and OC–Lumf (1 mg/mL) conjugates were prepared in complete culture media. Test compounds were diluted serially to concentrations ranging from 1 mg/mL to 0.002 mg/mL and added to cells in triplicate. Cells were incubated with the compounds for 24, 48, or 72 h. Phenylarsenic oxide (PAO) and DMSO served as positive and negative controls, respectively.

Following incubation, the medium was removed, cells were washed with PBS, and fresh unsupplemented medium was added. MTT (10 μL, 5 mg/mL) was added to each well and incubated for 3 h at room temperature. The medium was then discarded, and DMSO (100 μL) was added to dissolve formazan crystals. Absorbance was measured at 450 nm with a reference wavelength of 620 nm using an Infinite F500 microplate reader (Tecan, Switzerland). Each experiment was performed in duplicate for each incubation period.

2.3.2 | Immunofluorescent Imaging

Caco-2 cell cytoskeletal toxicity was assessed using an immunofluorescence assay. Cells were cultured in Opti-MEM supplemented with 5% FBS and 1% penicillin-streptomycin. They were seeded at densities of 5×10^4, 4×10^4, and 3×10^4 cells/well in 96-well plates and incubated for 24 h at 37°C in 5% CO_2.

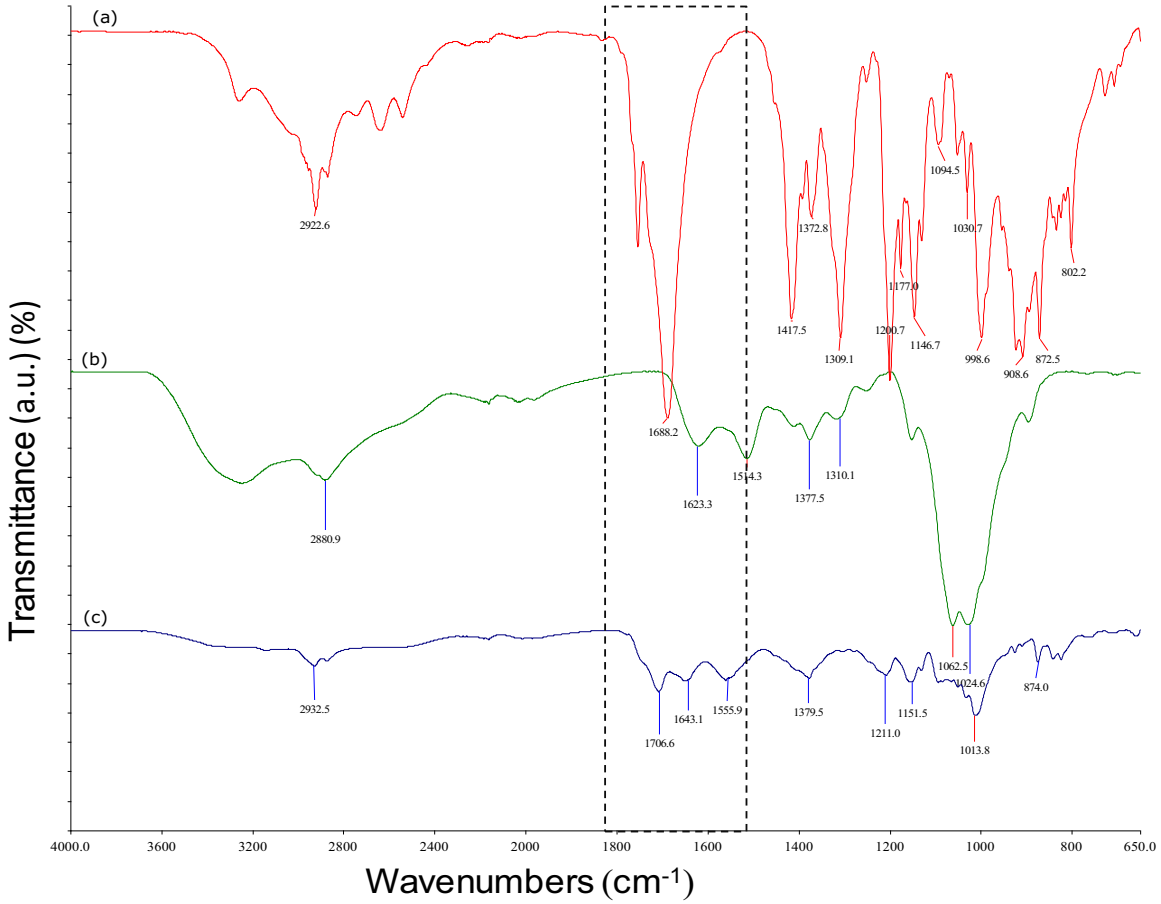

FIGURE 2 | FTIR spectra of (a) DHA-Suc, (b) OC, and (c) OC–DHA conjugate.

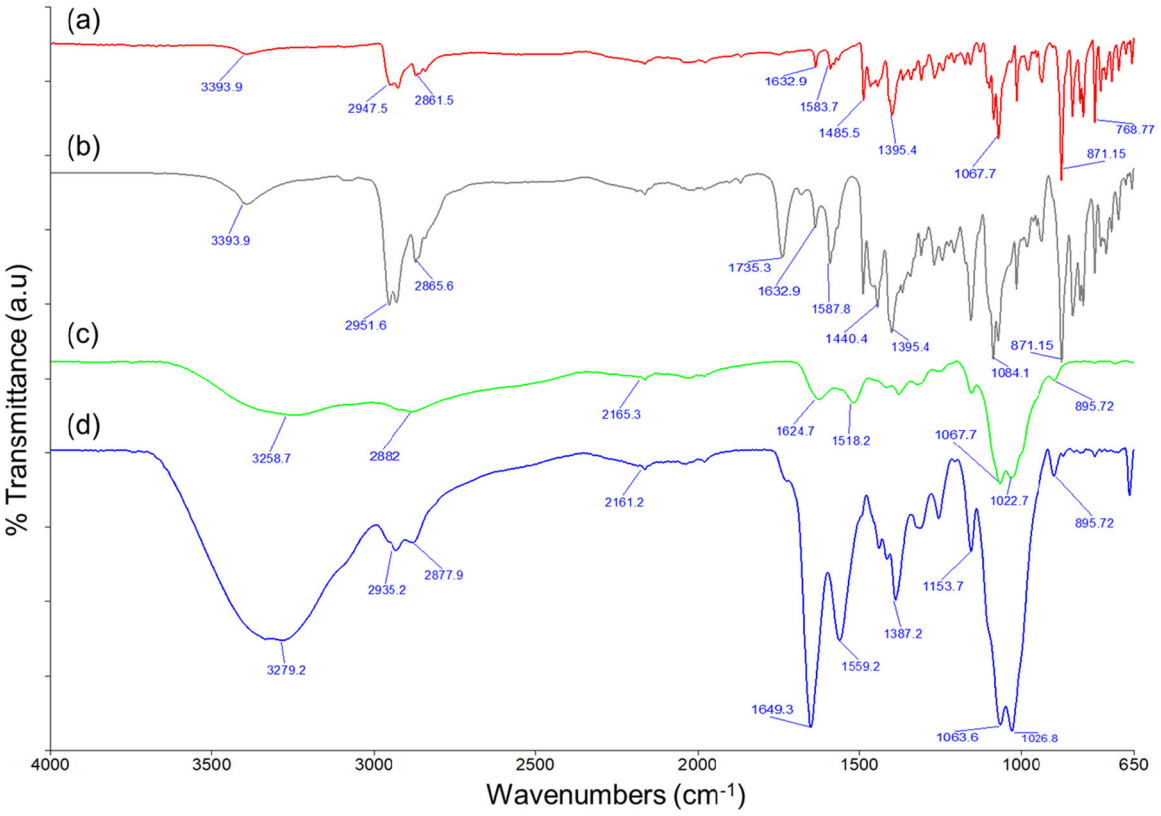

FIGURE 3 | FTIR spectra of (a) Lumf, (b) Lumf-Suc, (c) OC, and (d) OC–Lumf conjugate.

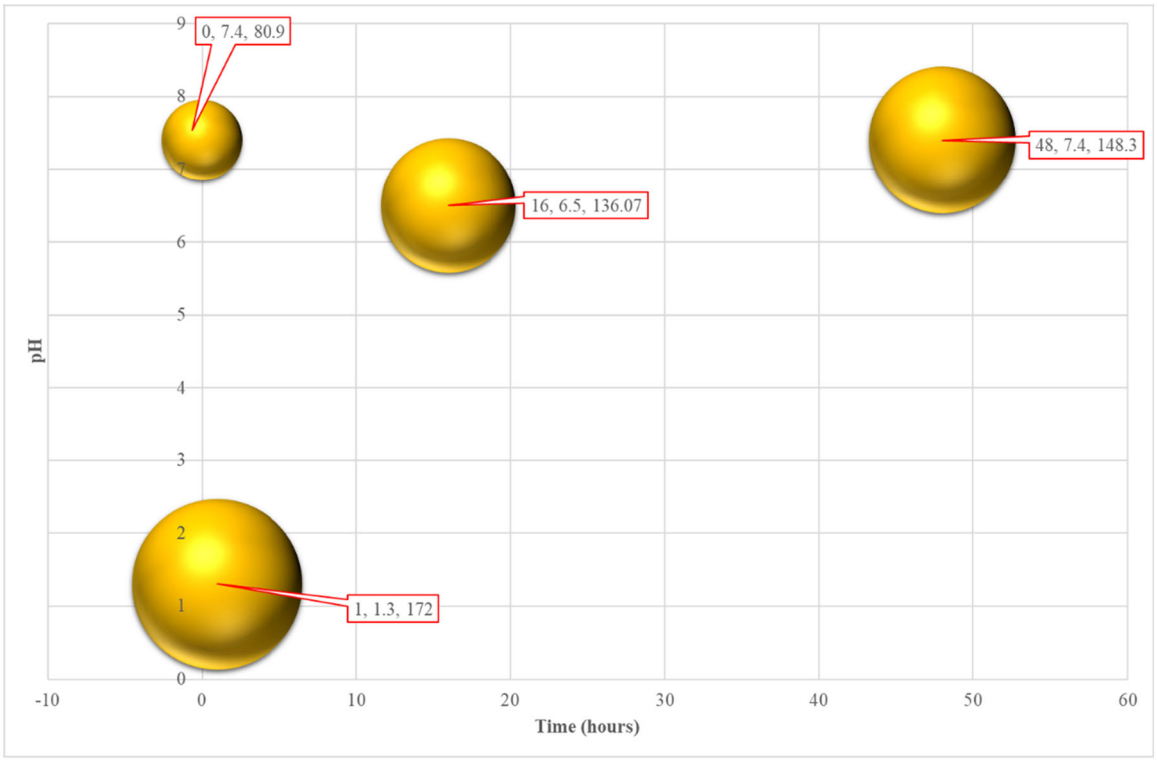

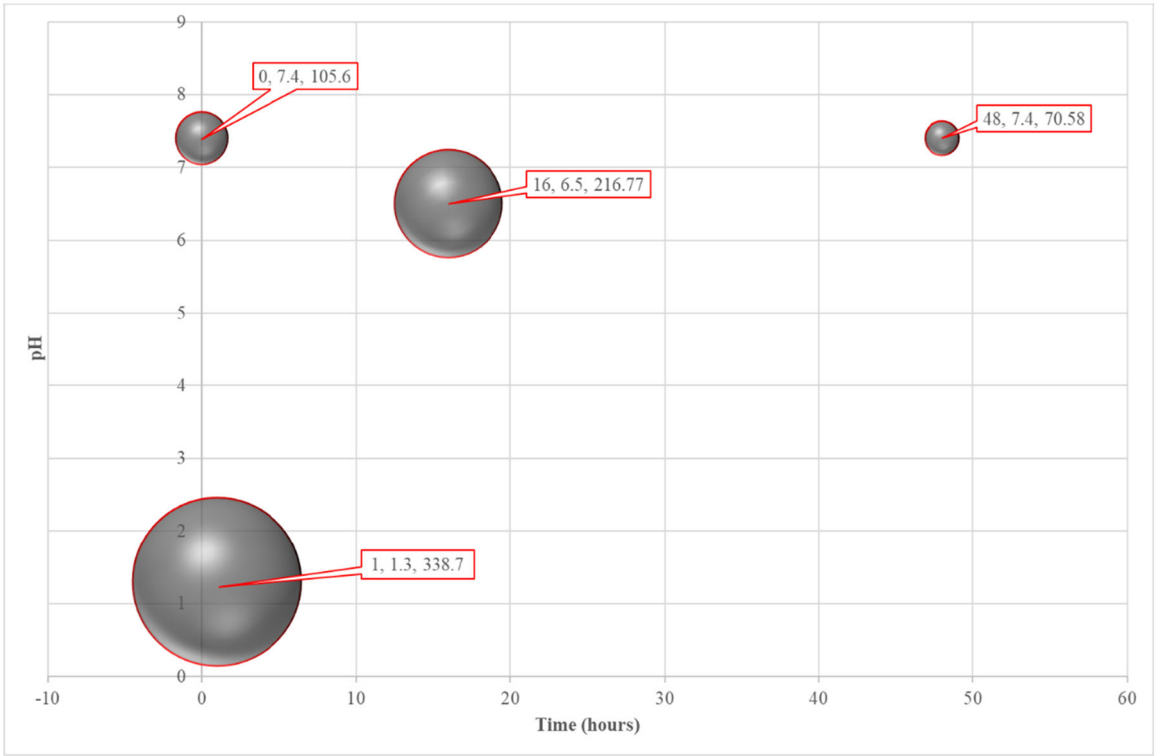

FIGURE 4 | Hydrodynamic properties of OC–DHA (top) and OC–Lumf (bottom) incubated at 37°C in aqueous solutions of pH 1.3, 6.5, and 7.4 over 48 h. Times are hours after the beginning of incubation at the specified pH. Refractive index: 1.520, absorption value: 0.001. (x, y, z) represent time, pH, d.nm.

After 24 h, cells were washed with PBS (100 mM, pH 7.2) and treated with free DHA, Lumf, OC–DHA, or OC–Lumf conjugates at concentrations ranging from 1 mg/mL to 0.002 mg/mL for 24, 48, or 72 h, respectively. Following incubation, cells were fixed with 4% paraformaldehyde for 10 min, permeabilized with 0.1% Triton X-100 for 10 min, and counterstained with Hoechst 33342 (12 μg/mL) for nuclear and ATTO 647 Phalloidin for actin cytoskeleton visualization. Cell images were acquired using a Cytation3 imaging reader (BioTek, the United States) at excitation/emission wavelengths of 405/400–450 nm for Hoechst 33342 and 635/650–670 nm for ATTO 647.

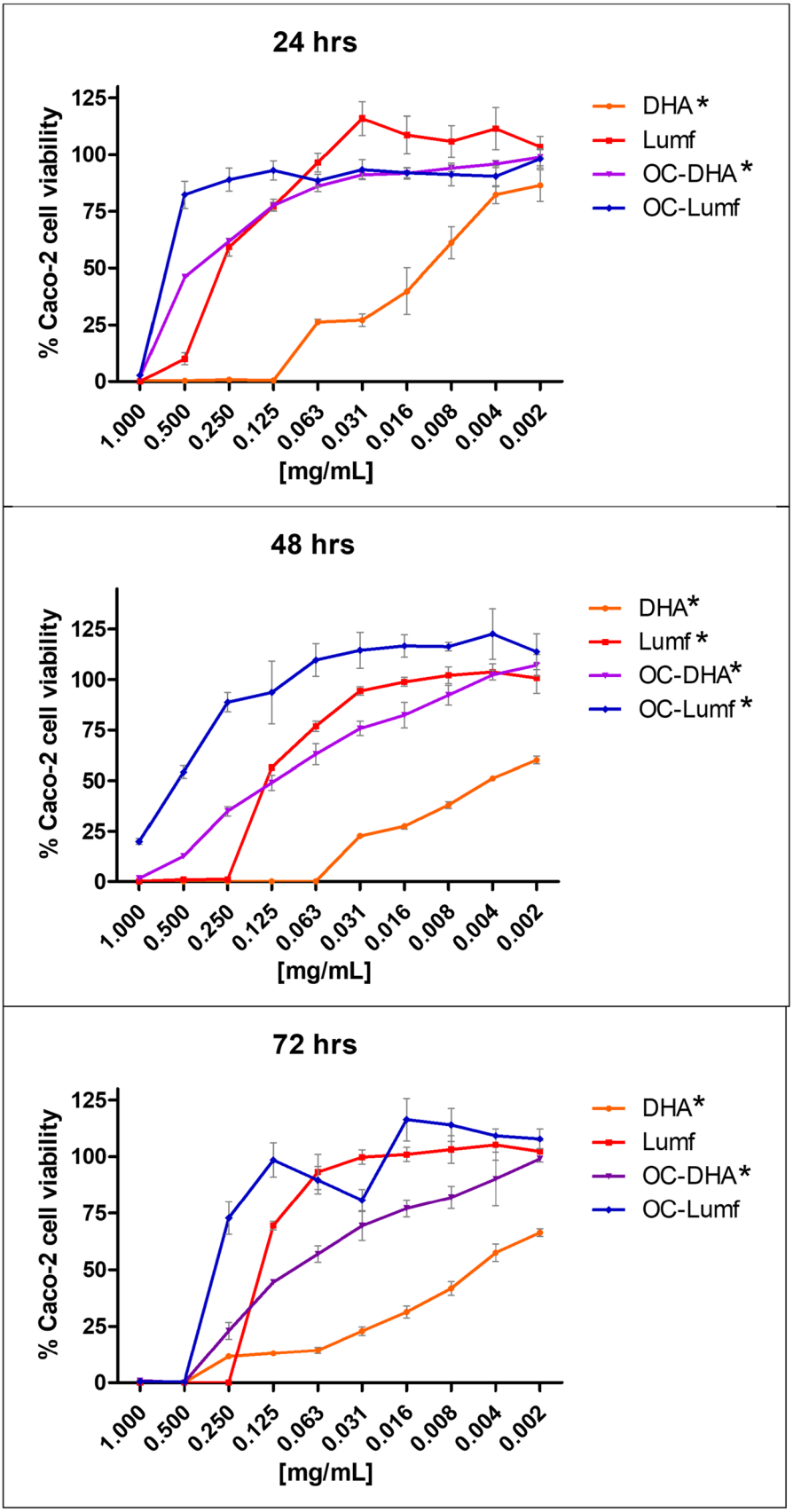

FIGURE 5 | Legend on next page.

2.4 | In Vitro Antiplasmodial Activity Screening

The antiplasmodial activity of OC conjugates was evaluated at the Malarial Parasite Molecular Laboratory (M^2PL) of the University of Pretoria, South Africa. *P. falciparum* NF54 strain was cultured at 37°C in human erythrocytes (O^+/A^+) suspended in complete culture medium (RPMI 1640 supplemented with 25 mM HEPES, 20 mM D-glucose, 200 μM hypoxanthine, 0.2% sodium bicarbonate, 24 μg/mL gentamicin, and 0.5% AlbuMax II) under a gas atmosphere of 90% N_2, 5% O_2, and 5% CO_2 as described by Verlinden et al. (2011) [39].

Ring stage parasites (1% hematocrit and 1% parasitemia) were treated with OC–DHA, OC–Lumf, free OC, DHA, and Lumf. Chloroquine phosphate (1 μM) and RPMI culture medium served as positive and negative controls, respectively. Cultures were incubated for 96 h at 37°C in 96-well plates under the specified gas atmosphere.

Following incubation, 100 μL of parasite culture was mixed with SYBR Green Lysis I buffer (0.2 μL/mL 10,000x SYBR Green I, Invitrogen; 20 mM Tris, pH 7.5; 5 mM EDTA; 0.008% saponin; 0.08% Triton X-100) and incubated for 1 h at room temperature. Fluorescence was measured using a GloMax-Explorer Detection System with Instinct Software (Promega Inc.) at excitation/emission wavelengths of 485/538 nm. Background fluorescence from chloroquine-treated samples was subtracted to isolate parasite-specific fluorescence.

Each experiment was performed in three technical replicates and three biological replicates ($n = 3$). Data analysis and graph generation were performed using Microsoft Excel and GraphPad Prism 7, respectively.

2.5 | Statistical Analysis

A paired *t*-test for two sample means was conducted for the in vitro biological data.

2.6 | Ethics

All in vitro biological experiments were conducted under approved protocols granted by the CSIR Research Ethics Committee (ref no.: 310/2020).

3 | Results and Discussion

3.1 | Spectroscopic Characterization of Purified Conjugates

Successful conjugation was confirmed by ^{1}H NMR spectroscopy. Signals corresponding to characteristic chemical shifts of Lumf and DHA were identified along with those of OC in the spectra of OC–Lumf and OC–DHA. FTIR also provided evidence of successful conjugation and was used to corroborate the ^{1}H NMR analyses.

3.1.1 | OC–DHA

^{1}H NMR spectroscopy analysis of DHA-Suc revealed the characteristic peaks of OC and DHA. The hexose ring's protons were visible at $\delta = 3.1–4.2$ ppm and the three equivalent protons of the acetyl group seen at $\delta = 1.90$ ppm (Figure 1). The proton peaks of DHA-Suc were observed at $\delta = 0.77–2.9$ ppm. The appearance of a new peak at $\delta = 8.32$ ppm, attributed to the secondary amide proton, confirmed the formation of an amide bond between OC and DHA-Suc.

The drug loading of the conjugate was calculated from the NMR signals to be 18 mol.%. This was done by comparing the ratio of integrated peaks of the hexose ring observed at 3.1–4.2 ppm to the methyl proton signals of DHA-Suc observed at 0.7–0.9 ppm and using the equation

$$\%DL = [(\text{drug proton signal})/(\text{polymer proton signal}) \times 1/3] \times 100.$$

FTIR spectroscopy further supported the successful conjugation (Figure 2). The appearance of absorption peaks at 1706.6 cm^{-1}, 1643.1 cm^{-1}, and 1555.9 cm^{-1}, corresponding to carbonyl (C=O) stretching and N-H bending vibrations, confirmed the formation of the amide bond.

3.1.2 | OC–Lumf

Confirmation by ^{1}H NMR spectroscopy of the successful conjugation of Lumf to OC was challenging because key diagnostic signals were obscured by the broader signals of the latter (Figure S3). However, a weak signal at 7.9 ppm in the OC–Lumf spectrum, corresponding to the aromatic protons of Lumf, provided some evidence of conjugation. The highly hydrophobic nature of Lumf may contribute to its encapsulation within a hydrophilic OC shell, further hindering the detection of its characteristic NMR signals.

The FTIR spectrum of OC–Lumf exhibited a significant shift in the amide I band from 1619 cm^{-1} (free OC) to 1645 cm^{-1}, indicating the formation of a new amide bond between OC and Lumf (Figure 3). Additionally, the disappearance of the carboxylic acid carbonyl peak at 1733 cm^{-1} in Lumf-Suc and its subsequent appearance at 1645 cm^{-1} in the conjugate further supported successful conjugation. The broad absorption band between 3000 and

FIGURE 5 | Concentration-dependent cytotoxicity in Caco-2 assay of OC–antimalarial conjugates. The free drugs and OC conjugates demonstrated significant toxicity at the highest concentration, 1.00 mg/mL, studied. Cell viability was more than 90% for OC, while the positive control, polyarsenic oxide, induced complete cell death. Data points are mean ± SD. *Statistically significant at p value < 0.05. *t*-test was conducted for free drug versus conjugate with a test of significance at p value < 0.05 for each of the incubation periods assuming equal variance between the sample time points of each test material. DHA versus OC–DHA was statistically significant at 24 h (p value = 0.0056), 48 h (p value = 0.0043), and at 72 h (p value = 0.0171). Lumf versus OC–Lumf was statistically significant only at 48 h (p value = 0.0418).

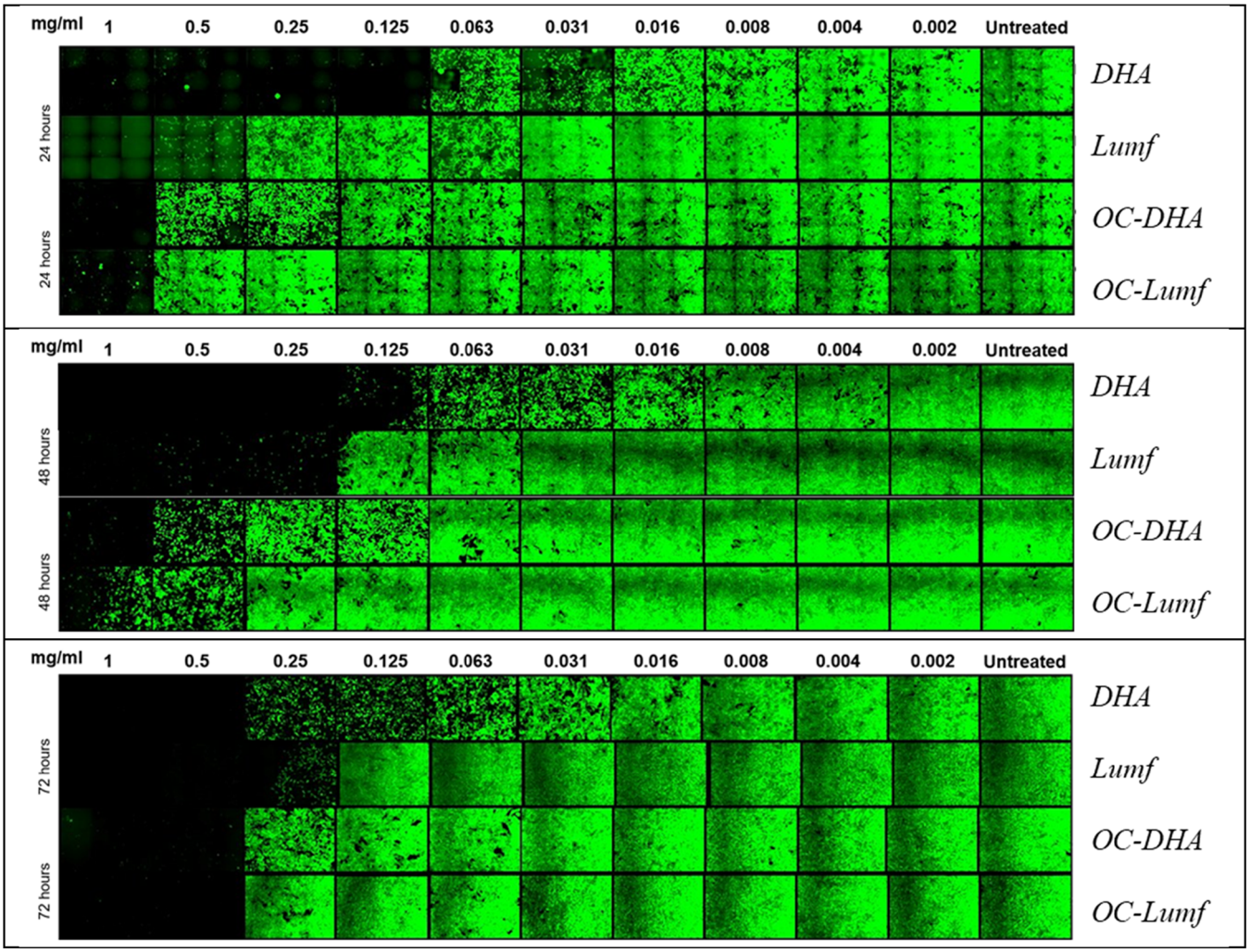

FIGURE 6 | Immunofluorescent assay of Caco-2 cells exposed to DHA, Lumf, and their OC conjugates. The images qualitatively illustrate the concentration-dependent responses of cells treated with the test compounds over 24, 48, and 72 h. Strong green fluorescence signifies high cell viability, whereas diminished or absent fluorescence indicates cell death.

$3600\,cm^{-1}$ in both the conjugate and the starting materials was attributed to O-H stretching vibrations.

The drug loading of OC–Lumf was determined by UV–Vis spectrophotometry on a Mettler Toledo UV5Bio spectrophotometer (Switzerland) at 335 nm according to the method described by Huang et al. 2010 (Figure S3) [40]. A standard curve ($R^2 = 0.9974$) of free Lumf was generated, and drug loading was found to be 112.39 μg/mg.

3.1.3 | Hydrodynamic Analysis

The OC–antimalarial drug conjugates were subjected to a series of pH solutions mimicking the stomach (pH 1.3), duodenum (pH 6.5), and the ileum and blood (pH 7.4). These are sections of the GIT with varying pH to which the OC conjugates would be exposed upon oral administration en route absorption into the blood. For both conjugates, particle size generally decreased over time (Figure 4). The initial DLS readings were taken at pH 7.4, which was used to stably dissolve the conjugates. The hydrodynamic diameter of OC–DHA was 105.6 ± 8.95 nm with a PDI of 0.276 ± 0.02 and a zeta potential of −18.70 mV, while OC–Lumf had a smaller initial particle size of 80.90 ± 4.06 nm with a PDI of 0.805 ± 0.132 and a zeta potential of −1.96 mV. The significantly low zeta potential of OC–Lumf conjugate indicates that its particles are highly susceptible to aggregation.

Upon lowering the pH to 1.3 and incubating for 1 h, the particle size of OC–DHA increased to 338.70 ± 54.55 nm, while the charge was all but completely lost (−0.024 mV). However, 16 h after the start of the experiment, and after raising the pH to 6.5, the particle size decreased to 216.77 ± 95.67 nm. Raising the pH again to 7.4 resulted in the observation of a further drop in diameter (Figure 4 top).

In contrast, OC–Lumf experienced a significant increase in particle size to 172.00 ± 63.90 nm, and zeta potential to −17.90 mV (Figure 4 bottom). Subsequent incubation at pH 6.5 and 7.4 only resulted in slightly lower particle sizes. The better size stability of OC–Lumf at different pH conditions can be attributed to the highly hydrophobic nature of Lumf, which may form a hydrophobic core within

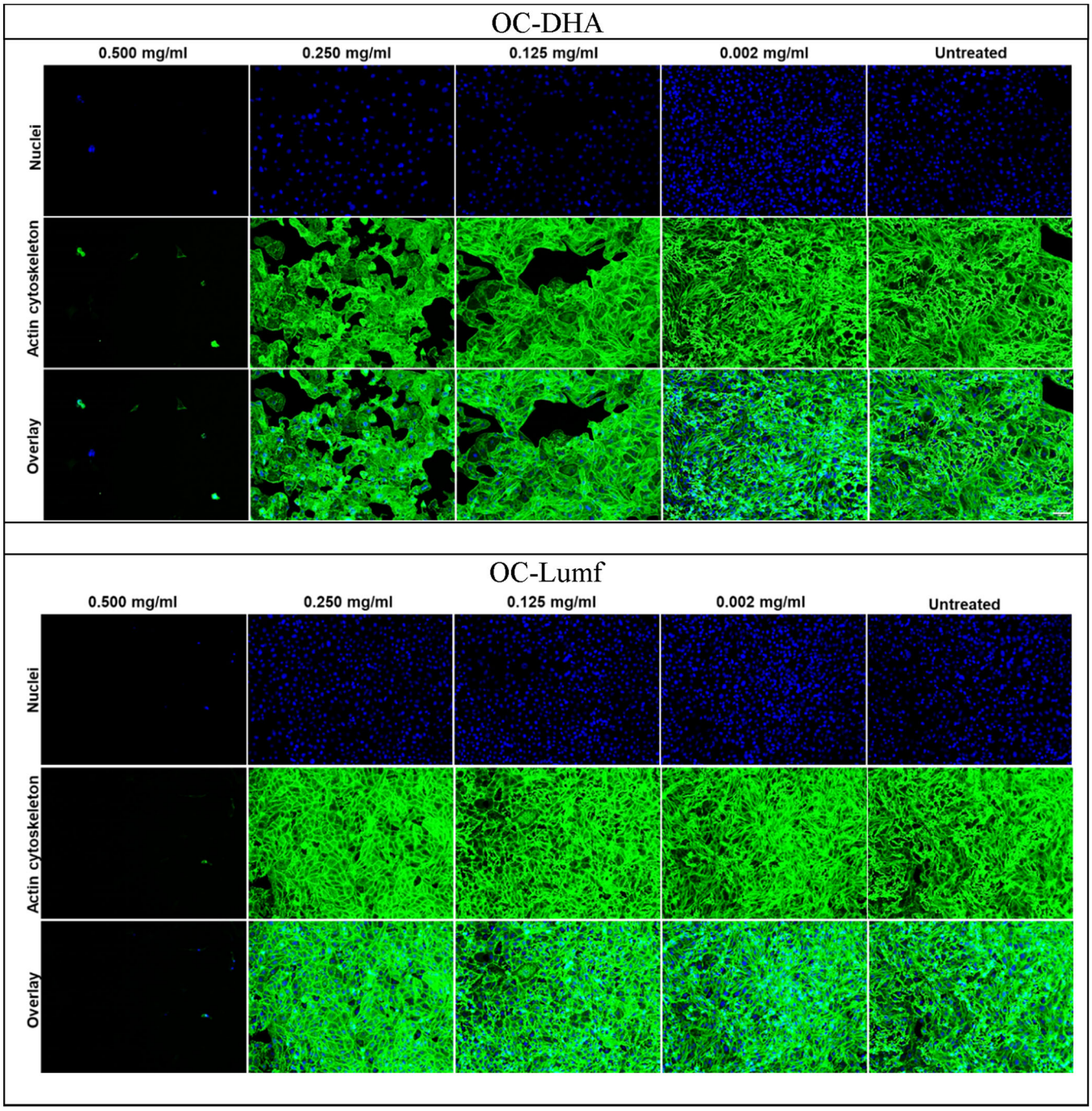

FIGURE 7 | Immunofluorescence staining of Caco-2 cells treated with various concentrations of OC–DHA (top) and OC–Lumf (bottom) and incubated for over 72 h. Green: actin cytoskeleton; Blue: nuclei. Scale bar: 100 μm.

a hydrophilic OC shell. This core formation can stabilize the particle size and prevent aggregation.

Without the stabilizing effects of crosslinkers and excipient surfactants, the conjugates exhibited sensitivity to pH changes. Acidic conditions initially caused particle aggregation, but prolonged exposure may have led to particle breakdown. The limited number of free amine groups in the OC may have been insufficient to induce significant electrostatic repulsion between particles, particularly in the presence of hydrophobic drugs.

3.2 | In Vitro Cytotoxicity

The cytotoxicity of OC–antimalarial drug conjugates was investigated with Caco-2 cells at 24, 48, and 72-h incubation periods (Figure 5). Caco-2 cells are an established in vitro model that mimics the intestinal epithelial lining. Similar toxicity profiles were observed at the three time periods studied. Both the free drugs (DHA and Lumf) and their OC conjugates (OC–DHA and OC–Lumf) demonstrated concentration-dependent cytotoxicity trends—as the concentration of these compounds increased, the percentage of viable cells decreased.

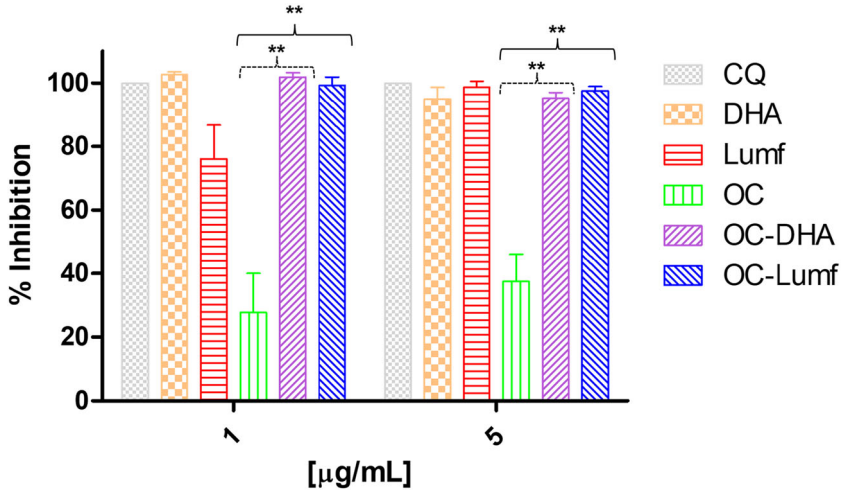

FIGURE 8 | In vitro antiplasmodial activity studies. The graph presents the percent inhibition of *P. falciparum* growth at two different concentrations (1 and 5 μg/mL) for the OC–antimalarial conjugates (OC–DHA and OC–Lumf), the free drugs (DHA and Lumf), OC, and chloroquine (CQ). Data points are mean ± SEM. $^{**}p$ value < 0.001.

While cell viability was very poor with DHA exposure even at 16 μg/mL, viability due to Lumf exposure decreased sharply below 50% only above 0.25 mg/mL. Conjugation to OC appears to have ameliorated the drug toxicities with both OC–DHA and OC–Lumf exhibiting reduced cytotoxicity compared to their respective free drug forms. Due to covalent binding to OC, the drugs are less available for burst-release exposure of the cells; there is rather a controlled stimulus-responsive release under appropriate conditions, for example, the low pH of the endolysosomal vesicles [41].

The significant differential toxicity observed between the free DHA and Lumf was also observed between the conjugates. Cells exposed to OC–Lumf consistently showed a greater tolerance to the conjugate compared to OC–DHA. DHA's higher toxicity may be attributed to the production of free radicals from the redox cleavage of its endoperoxide bridge, which can also occur even without the release of the drug from the conjugate [42, 43]. These free radicals can damage cellular components and lead to cell death.

Like the observations after 24 h, all the test compounds continue to show a concentration-dependent decrease in Caco-2 cell viability at 48 and 72 h, but with generally more pronounced toxicity. Pristine OC did not induce any significant concentration-dependent toxicity (Figure S5). While the conjugation of the drugs to OC mitigates the toxicity of the drugs, prolonged exposure erodes this effect in a time-dependent trend, as observed with OC–Lumf. These findings highlight the importance of optimizing the dosage and administration regimen of OC–antimalarial drug conjugates to minimize potential side effects while maximizing therapeutic efficacy.

3.2.1 | Immunofluorescent Imaging

The concentration-dependent effects of the conjugates were visualized through immunofluorescent imaging of the cells (Figure 6). The advantage of OC conjugation was evident, with clearly discernible green fluorescence indicating significant cellular activity at 0.5 mg/mL after the initial 24-h exposure period for both conjugates. The most significant difference in cytotoxicity was observed with DHA, as was the case with the cell proliferation studies. Cells exposed to as little as 0.125 mg/mL of free DHA showed almost no cellular activity. In contrast, cells that were treated with OC–DHA emitted a strong green fluorescence, which was indicative of thriving cellular activity even at a 0.5 mg/mL dose treatment.

At the 72-h endpoint, all treatment groups exposed to concentrations of 0.25 mg/mL or less demonstrated significant recovery of cellular activity. Cellular proliferation observed in free drug-treated assays may be attributed to molecular degradation of the compounds, particularly the labile endoperoxide bridge of DHA. After 72 h of incubation, minimal evidence of viable cells remained at concentrations of 0.5 mg/mL and 1.0 mg/mL for both free and conjugated drug formulations. This noticeable increase in cytotoxicity of OC–DHA and OC–Lumf may be due to conjugate degradation, resulting in the release of still potent drug molecules.

We also investigated the concentration-dependent toxicity of the conjugates on the nuclei and actin cytoskeletons of Caco-2 cells to understand the underlying subcellular causes of the cytotoxicity. In untreated cells, well-organized actin cytoskeletons with distinct filamentous structures and intact nuclei were observed (Figure 7). However, a progressive loss of cell morphology was noted, with distinct dose-dependent cellular damage occurring in both OC–DHA and OC–Lumf-treated cells. At 0.5 mg/mL, the actin cytoskeletons lost their filamentous structures, appearing fragmented and disorganized. The nuclei also became fragmented and condensed, indicating cell death. In comparison, a more profound damage to these subcellular components was observed in cells treated with the free drugs and at significantly lower doses (Figure S4). Further studies are required to elucidate the precise mechanisms underlying these effects.

3.3 | In Vitro Antiplasmodial Activity

Like the free drugs, the inhibition of *P. falciparum* growth at 1 μg/mL and 5 μg/mL for the OC–antimalarial drug conjugates was

dose-dependent (Figure 8). There was a clearly demonstrable enhancement in activity of the OC–Lumf and OC–DHA conjugates compared to their respective free drugs, suggesting that conjugation to OC offers an improvement in the antiplasmodial efficacy of these drugs. OC–Lumf produced the greatest enhancement in potency, showing $99.27 \pm 2.54\%$ inhibition of parasite growth even at the lower test concentration of 1 μg/mL, whereas the free Lumf was $76.00 \pm 10.64\%$ (z-factor = 0.91) effective.

The observed enhancement in antiplasmodial activity with the conjugates may be attributable to improved cellular uptake of the drug molecules, facilitated by OC's membrane adhesiveness, leading to increased intracellular concentrations and parasite killing. Additionally, the sustained release of the drugs from the OC carrier may prolong their activity and improve efficacy. The combination of OC and the antimalarial drug may also have a significant synergistic effect, with the polymer demonstrating measurable inhibitory activity of $27.76 \pm 12.23\%$ and $37.40 \pm 8.62\%$ for the 1 μg/mL and 5 μg/mL test concentrations, respectively. Interestingly, while the pristine OC exhibited a large and measurable toxicity to the *P. falciparum* cells, the same effect was not measurable in human Caco-2 cells, even at concentrations 200–1000 times higher than those to which the parasite was exposed (Figure S5). Previous reports have described the cytoprotective effects of Cs [44]. That this was not observed in this study with *P. falciparum* could suggest that OC may be selectively active against the parasite, potentially due to differences in cellular uptake or metabolic pathways.

4 | Conclusion

Both DHA and Lumf have relatively safe and tolerability profiles in humans, and the conjugation to OC did not introduce any new cytotoxicity. We have demonstrated the potential of OC as a polymeric carrier for the antimalarial drugs Lumf and DHA. By employing a combination of spectroscopic techniques, quantitative cell viability and immunofluorescence microscopy, and antiplasmodial assays, we acquired comprehensive initial experimental data on the activity of OC conjugates of these antimalarial drugs. Both conjugates demonstrated improved cell tolerance and viability compared to the free drugs. Notably, the OC conjugates maintained comparable antiplasmodial efficacy to the free drugs.

Particle size significantly impacts the biological performance of drug delivery systems. We observed that hydrodynamic properties, such as diameter, charge, and polydispersity of the OC–drug conjugates, were erratically influenced by pH conditions like those encountered along the GIT after oral administration. By optimizing the formulation of the conjugates through deliberate particle engineering, it may be possible to enhance their stability.

Acknowledgements

The authors would like to thank the World Health Organization (WHO) and the South African Medical Research Council (SAMRC) through the CEWG Demonstration project grant and the National Research Foundation (NRF) (grant numbers: 104907 and 114369) for financial support. The University of Pretoria provided postdoctoral funding to I.M.F. The Malarial Parasite Molecular Laboratory (M^2PL) of the University of Pretoria conducted the antiplasmodial testing as a paid service.

Conflicts of Interest

The authors declare no conflicts of interest.

Data Availability Statement

The data that support the findings of this study are available from the corresponding author upon reasonable request.

References

1. S. Mvango, W. M. R. Matshe, A. O. Balogun, L. A. Pilcher, and M. O. Balogun, "Nanomedicines for Malaria Chemotherapy: Encapsulation vs. Polymer Therapeutics," *Pharmaceutical Research* 35 (2018): 237, http://link.springer.com/10.1007/s11095-018-2517-z.

2. World Malaria Report 2023. World Health Organization. 2023.

3. World Health Organization. Guidelines for the Treatment of Malaria. 2015.

4. B. M. Gruessner, L. Cornet-Vernet, M. R. Desrosiers, P. Lutgen, M. J. Towler, and P. J. Weathers, "It Is Not Just Artemisinin: *Artemisia* sp. for Treating Diseases Including Malaria and Schistosomiasis," *Phytochemistry Reviews* 18 (2019): 1509–1527.

5. D. Zheng, T. Liu, S. Yu, Z. Liu, J. Wang, and Y. Wang, "Antimalarial Mechanisms and Resistance Status of Artemisinin and Its Derivatives," *Tropical Medicine and Infectious Disease* 9, no. 223 (2024): 39330912, https://doi.org/10.3390/tropicalmed9090223.

6. O. P. S. Patel, R. M. Beteck, and L. J. Legoabe, "Exploration of Artemisinin Derivatives and Synthetic Peroxides in Antimalarial Drug Discovery Research," *European Journal of Medicinal Chemistry* 213 (2021): 113193.

7. M. Azman, A. H. Sabri, Q. K. Anjani, M. F. Mustaffa, and K. A. Hamid, "Intestinal Absorption Study: Challenges and Absorption Enhancement Strategies in Improving Oral Drug Delivery," *Pharmaceuticals* 15 (2022): 15080975.

8. S. S. Jambhekar and P. J. Breen, "Drug Dissolution: Significance of Physicochemical Properties and Physiological Conditions," *Drug Discovery Today* 18 (2013): 1173–1184.

9. K. Na-Bangchang and J. Karbwang, "Pharmacology of Antimalarial Drugs, Current Anti-malarials." *Encyclopedia of Malaria* (Springer, 2019), 1–82.

10. E. A. Ashley, K. Stepniewska, N. Lindegårdh, et al., "How Much Fat Is Necessary to Optimize Lumefantrine Oral Bioavailability?," *Tropical Medicine & International Health* 12, no. 2 (February, 2007): 195–200.

11. U. K. Baruah, K. Gowthamarajan, R. Vanka, V. V. S. R. Karri, K. Selvaraj, and G. M. Jojo, "Malaria Treatment Using Novel Nano-Based Drug Delivery Systems," *Journal of Drug Targeting* 25, no. 7 (2017): 567–581.

12. M. O. Balogun, J. O. Akolade, and A. O. Balogun, "Chapter 8. Development of Nanocarriers for Innovative Antimalarial Combination Strategies," in *Applications of Nanobiotechnology for Neglected Tropical Diseases, ed. F. R. Formiga and Severino P. Inamuddin* (Elsevier, 2021), 141–167.

13. P. Ghasemiyeh and S. Mohammadi-Samani, "Solid Lipid Nanoparticles and Nanostructured Lipid Carriers as Novel Drug Delivery Systems: Applications, Advantages and Disadvantages," *Research in Pharmaceutical Sciences* 13 (2018): 235156.

14. P. A. Odera, G. Otieno, J. O. Onyango, et al., "Nanoparticle-Based Formulation of Dihydroartemisinin-Lumefantrine Duo-Drugs: Preclinical Evaluation and Enhanced Antimalarial Efficacy in a Mouse Model," *Heliyon* 10, no. 6 (March 30, 2024): e26868.

15. A. Garg, K. Bhalala, D. S. Tomar, and Wahajuddin, "In-Situ Single Pass Intestinal Permeability and Pharmacokinetic Study of Developed Lumefantrine Loaded Solid Lipid Nanoparticles," *International Journal*

of Pharmaceutics 516, no. 1–2 (2017): 120–130, https://doi.org/10.1016/j.ijpharm.2016.10.064.

16. P. Prabhu, S. Suryavanshi, S. Pathak, S. Sharma, and V. Patravale, "Artemether–Lumefantrine Nanostructured Lipid Carriers for Oral Malaria Therapy: Enhanced Efficacy at Reduced Dose and Dosing Frequency," *International Journal of Pharmaceutics* 511, no. 1 (2016): 473–487.

17. P. Prabhu, S. Suryavanshi, S. Pathak, A. Patra, S. Sharma, and V. Patravale, "Nanostructured Lipid Carriers of Artemether–Lumefantrine Combination for Intravenous Therapy of Cerebral Malaria," *International Journal of Pharmaceutics* 513, no. 1–2 (2016): 504–517.

18. D. Mehtani, A. Seth, P. Sharma, et al., "Biomaterials for Sustained and Controlled Delivery of Small Drug Molecules," *Biomaterials and Bionanotechnology* (January 1, 2019): 89–152.

19. N. Islam, I. Dmour, and M. O. Taha, "Degradability of Chitosan Micro/Nanoparticles for Pulmonary Drug Delivery," *Heliyon* 5 (2019): e01684.

20. N. Desai, D. Rana, S. Salave, et al., "Chitosan: A Potential Biopolymer in Drug Delivery and Biomedical Applications," *Pharmaceutics* 15 (2023): 15041313.

21. K. A. Janes, P. Calvo, and M. J. Alonso, "Polysaccharide Colloidal Particles as Delivery Systems for Macromolecules," *Advanced Drug Delivery Reviews* 47 (2001), www.elsevier.com/locate/drugdeliv.

22. B. B. M. Garcia, S. Douka, O. Mertins, E. Mastrobattista, and S. W. Han, "Efficacy of Chitosan-N-Arginine Chitosomes in mRNA Delivery and Cell Viability Enhancement," *ACS Applied Bio Materials* 7 (2024): 8261–8271.

23. K. Jafernik, A. Ładniak, E. Blicharska, et al., "Chitosan-Based Nanoparticles as Effective Drug Delivery Systems—A Review," *Molecules* 28 (2023): 28041963.

24. M. A. Mohammed, J. T. M. Syeda, K. M. Wasan, and E. K. Wasan, "An Overview of Chitosan Nanoparticles and Its Application in Non-Parenteral Drug Delivery," *Pharmaceutics* 9 (2017): 9040053.

25. F. Gomes, A. C. Ribeiro, G. S. Sanches, et al., "A Nanochitosan-D-Galactose Formulation Increases the Accumulation of Primaquine in the Liver," *Antimicrobial Agents and Chemotherapy* 68, no. 5 (May 1, 2024): 00915-23.

26. I. Karakurt, K. Ozaltin, E. Vargun, et al., "Controlled Release of Enrofloxacin by Vanillin-Crosslinked Chitosan-Polyvinyl Alcohol Blends," *Materials Science and Engineering: C* 126 (July 1, 2021): 112125.

27. Z. Cele, L. Ndlandla, A. Somboro, D. Gyamfi, and M. Balogun, "Synthesis, Characterization and Antimicrobial Activities of Quaternary Chitosan-Based Materials," in IOP Conference Series: Materials Science and Engineering (2018), 012048, http://stacks.iop.org/1757-899X/430/i=1/a=012048?key=crossref.a0125da18f7d0283564e55877517750c.

28. Z. E. D. Cele, W. Matshe, L. Mdlalose, et al., "Cationic Chitosan Derivatives for the Inactivation of HIV-1 and SARS-CoV-2 Enveloped Viruses," *ACS Omega* 8, no. 35 (September 5, 2023): 31714–31724.

29. W. M. R. Matshe, L. Tshweu, and M. O. Balogun, "Synthesis of a Novel Amphiphilic Nano-Chitosan Material," in *IOP Conference Series: Materials Science and Engineering* (2018).

30. K. H. Min, K. Park, Y. S. Kim, et al., "Hydrophobically Modified Glycol Chitosan Nanoparticles-Encapsulated Camptothecin Enhance the Drug Stability and Tumor Targeting in Cancer Therapy," *Journal of Controlled Release* 127, no. 3 (May 8, 2008): 208–218.

31. L. Hu, Y. Sun, and Y. Wu, "Advances in Chitosan-Based Drug Delivery Vehicles," *Nanoscale* 5 (2013): 3103–3111.

32. E. Lee, H. Kim, I. H. Lee, and S. Jon, "In Vivo Antitumor Effects of Chitosan-Conjugated Docetaxel After Oral Administration," *Journal of Controlled Release* 140, no. 2 (2009): 79–85.

33. E. Lee, J. Lee, I. H. Lee, et al., "Conjugated Chitosan as a Novel Platform for Oral Delivery of Paclitaxel," *Journal of Medicinal Chemistry* 51, no. 20 (2008): 6442–6449.

34. S. Y. Chae, M. K. Jang, and J. W. Nah, "Influence of Molecular Weight on Oral Absorption of Water Soluble Chitosans," *Journal of Controlled Release* 102, no. 2 (February 2, 2005): 383–394.

35. W. M. R. Matshe, L. L. Tshweu, S. Mvango, et al., "A Water-Soluble Polymer-Lumefantrine Conjugate for the Intravenous Treatment of Severe Malaria," *Macromolecular Bioscience* 23, no. 5 (May 1, 2023): 0.

36. S. Alven, B. A. Aderibigbe, M. O. Balogun, W. M. R. Matshe, and S. S. Ray, "Polymer-Drug Conjugates Containing Antimalarial Drugs and Antibiotics," *Journal of Drug Delivery Science and Technology* 53 (2019): 101171, https://doi.org/10.1016/j.jddst.2019.101171.

37. L. Neves Borgheti-Cardoso, M. San Anselmo, E. Lantero, et al., "Promising Nanomaterials in the Fight Against Malaria," *Journal of Materials Chemistry. B* 8, no. 41 (November 7, 2020): 9428–9448.

38. D. Xiao, B. Yang, X. M. Yang, et al., "Synthesis of Water Soluble Chitosan-Artemisinin Conjugate," *Asian Journal of Chemistry* 25, no. 8 (2013): 4637–4639.

39. B. K. Verlinden, J. Niemand, J. Snyman, et al., "Discovery of Novel Alkylated (Bis)Urea and (Bis)Thiourea Polyamine Analogues With Potent Antimalarial Activities," *Journal of Medicinal Chemistry* 54, no. 19 (October 13, 2011): 6624–6633.

40. L. Huang, P. S. Lizak, A. L. Jayewardene, et al., "A Modified Method for Determination of Lumefantrine in Human Plasma by HPLC-UV and Combination of Protein Precipitation and Solid-Phase Extraction: Application to a Pharmacokinetic Study," *Analytical Chemistry Insights* 5 (2010): 15–23.

41. R. Duncan, "Designing Polymer Conjugates as Lysosomotropic Nanomedicines," *Biochemical Society Transactions* 35 (2007): 56–60, http://www.esf.org/.

42. P. Zhu and B. Zhou, "The Antagonizing Role of Heme in the Antimalarial Function of Artemisinin: Elevating Intracellular Free Heme Negatively Impacts Artemisinin Activity in *Plasmodium falciparum*," *Molecules* 27, no. 6 (March 1, 2022): 1755.

43. H. C. Quadros, M. C. B. Silva, and D. R. M. Moreira, "The Role of the Iron Protoporphyrins Heme and Hematin in the Antimalarial Activity of Endoperoxide Drugs," *Pharmaceuticals* 15 (2022): 15010060.

44. F. N. Maluin, M. Z. Hussein, N. A. Yusof, et al., "Cytoprotection, Genoprotection, and Dermal Exposure Assessment of Chitosan-Based Agronanofungicides," *Pharmaceutics* 12, no. 6 (June 1, 2020): 497.

Supporting Information

Additional supporting information can be found online in the Supporting Information section.
Final_SupplementaryInformation.